Assessing the Net Climate Impact of Norwegian Reservoirs: Integrating Land Use Change and G-res Modeling

Kenawi, Mahmoud S.[1*] Hedger, Richard D.[2] Keymasi, Mobina[3] Vakhidi, Fabian[1] , Gotsiridze, Elene[1] Alfredsen, Knut T.[1], Sandercock, Brett K.[2] Silvennoinen, Hanna M.[2] Bakken, Tor H.[1]

1 Department of Civil and Environmental Engineering, Norwegian University of Science and Technology, Trondheim, Norway

2 Norwegian Institute for Nature Research (NINA), Trondheim, Norway

3 Research Center for Spatial Information (CEOSpaceTech), The National University of Science and Technology POLITEHNICA Bucharest, Bucharest, Romania

***Correspondence**: Mahmoud Saber Kenawi

Email: mahmoud.s.kenawi@ntnu.no

Address: S. P. Andersens veg 5, 7031 Trondheim, Norway

Preprint status:

This manuscript is a non-peer-reviewed preprint submitted to EarthArXiv. The manuscript is currently under review at Journal of Water and Climate Change.

Abstract

This study evaluates the net climate impact of Norwegian reservoirs using land use change mapping, literature-based GHG flux aggregation, and G-res modeling. High-resolution historical aerial imagery and deep learning reconstructed pre-impoundment land cover, explicitly identifying wetlands previously absent from national datasets. The framework quantifies changes in CO_2 and CH_4 fluxes and cumulative GWP_{100} across 52 reservoirs. Wetlands made up 20% of pre-flooded land and strongly influenced carbon dynamics. Boreal wetland fluxes produced net emissions of 342 ± 40 g CO_2-eq m^{-2} yr^{-1}, driven mainly by CH_4 despite notable CO_2 sequestration. GWP_{100} values ranged from -260 to 217 kt CO_2-eq, showing high spatial variability linked to pre-flood soil and land cover. Hydropower GHG intensity averaged 0.19 g CO_2-eq kWh^{-1}, lower than global estimates due to low productivity and rapid water turnover. Future research should improve soil classification, expand boreal flux datasets, and develop process-based models for pre- and post-impoundment carbon dynamics.

Keywords

Hydropower, Greenhouse Gas, Land use change, Remote Sensing, Reservoirs

Highlights

- **Wetlands comprised 20% (103 km^2) of pre-impoundment land across 52 reservoirs**
- **Boreal wetlands emitted 342 ± 40 g CO_2-eq m^{-2} yr^{-1}, dominated by CH_4 fluxes**
- **Pre-development fluxes varied from −1,470 to 3,981 t CO_2-eq yr^{-1}**
- **Reservoir net GWP_{100} ranged from −260 to 217 kt CO_2-eq**
- **Mean hydropower emission intensity was 0.19 g CO_2-eq kWh^{-1}**

1 Introduction

Climate change represents a major global challenge, driven by increasing greenhouse gas (GHG) emissions from anthropogenic activities that alter temperature regimes and precipitation patterns (Jia et al., 2022). Land use (LU) and land use change (LUC) contribute substantially to these emissions, accounting for approximately 23% of total anthropogenic sources (IPCC, 2022). The conversion of natural ecosystems such as forests, wetlands, and grasslands diminishes carbon storage capacity and disrupts biogeochemical processes.

Reservoirs provide vital services that support socio-economic development and environmental management. They may provide multiple services, such as reliable water storage for domestic water supply, agricultural and industrial use, control floods and provide flow for navigation, serve important recreational activities and ecological habitats, and provide storage for hydropower production. Moreover, hydropower generation supplies approximately 18% of global electricity (IEA, 2021), representing a cornerstone of renewable energy production and a key component of low-carbon transition strategies. As global energy demand grows and decarbonization efforts intensify, the strategic role of reservoirs in sustainable resource management and climate mitigation has gained increasing attention, particularly as hydropower with reservoirs remains the only large-scale technology capable of providing the flexibility needed to balance intermittent solar and wind power across time scales from seconds to months.

Despite their benefits, reservoir creation and operation induce substantial environmental changes that influence GHG dynamics (Kumar et al., 2023). The inundation of terrestrial ecosystems transforms natural carbon cycling, shifting from predominantly aerobic decomposition processes before flooding to anaerobic conditions post-inundation (Li & Zhang, 2014). This transition leads to the production and emission of Carbon dioxide (CO_2) and Methane (CH_4), which vary in magnitude depending on climatic conditions, reservoir morphometry, and the characteristics of the flooded landscape. Pre- and post-inundation emissions differ not only in their pathways but also in their temporal persistence, often continuing for years or decades after impoundment (Bertassoli et al., 2021; Rodriguez & Casper, 2018). However, uncertainties remain regarding the quantification of these emissions, as current estimation methods and measurement tools are limited in spatial coverage and methodological consistency (Kumar et al., 2023). Addressing these knowledge gaps is essential for accurately assessing the net GHG balance of reservoirs within the broader context of LUC and climate policy.

In Norway, where approximately 85% of electricity installed capacity is from hydropower (OED, 2022), reservoirs are central to national energy production, environmental management, and flood control. The country holds over 2,700 reservoirs covering more than 8,000 km^2 (NVE, 2023), underscoring the pivotal role of hydropower in its renewable energy strategy. However, despite their extensive development and environmental significance, few studies have quantified the GHG emissions associated with Norwegian reservoirs. The inundation of terrestrial ecosystems during reservoir formation alters natural carbon cycling and can release CO_2 and CH_4 through aerobic and anaerobic processes. Understanding and accurately estimating these emissions are essential for assessing the true climate impact of hydropower systems and ensuring that Norway's renewable energy goals align with its long-term commitments to emission reduction and climate neutrality.

To address the knowledge gap between reservoir development and associated GHG impacts in boreal regions, it is essential to first determine the types of LU converted during reservoir construction. In the boreal landscapes of Norway, previous work by Kenawi et al. (2023) successfully classified land types for 108 reservoirs which represented approximately 12% of the total reservoir surface area in the country. The work utilized historical aerial imagery, textural features, and object-based image analysis (OBIA). Kenawi et al. (2023) established a crucial foundation for assessing the spatial extent and environmental characteristics of inundated boreal ecosystems influenced by hydropower development. However, methodological limitations prevented the accurate identification of wetlands as a distinct land class, despite their critical role in carbon storage and cycling. Furthermore, the analysis did not establish any direct associations between LU transitions and corresponding GHG emissions from the studied reservoirs. Addressing these gaps through improved classification techniques and emission measurements is essential for accurately quantifying the carbon implications of hydropower development and advancing Norway's efforts toward sustainable energy and climate goals.

Building on that, the goal of this study is to enhance the understanding of the relationship between LUC and reservoir development in Norway to provide insights that can support policymakers in assessing the net GHG emissions associated with future reservoir developments or expansions. Building upon the previous analysis conducted by Kenawi et al. (2023), which focused on identifying land types associated with reservoirs, this study aims to:

i) Expand and refine LUC analyses of Norwegian reservoirs by integrating wetlands into existing classifications of converted land types using high-resolution spatial data.

ii) Quantify pre-development GHG fluxes (CO_2 and CH_4) for identified ecosystems by aggregating annual emissions and sinks per land type, derived from field and remote sensing data.

iii) Estimate post-development GHG emissions by applying the G-res tool to reservoir-specific conditions, accounting for temporal variation and calculating net global warming potential of the 100 years period (GWP100) by comparing these emissions with pre-impoundment baselines.

iv) Determine the GHG intensity (gCO_2eq/kWh) of each reservoir by annual net emissions to the electricity output of the associated hydropower scheme.

2 Data and Methods

The approach of achieving this study objectives builds on three interconnected components that together provide a consistent framework for assessing the net GHG consequences of reservoir developments in the boreal region. First, high-resolution remote sensing data and aerial imagery were used to establish a detailed baseline of pre-development land cover, with particular emphasis on the explicit identification of wetlands. This refined classification extends the work of Kenawi et al. (2023) and provides the spatial foundation for subsequent emission accounting.

Second, available measurements of net ecosystem exchange (NEE) which define the net balance between the absorbed and sequestered CO_2 and CH_4 fluxes which were derived from field studies, monitoring networks, and remote sensing products. The measurements were compiled and harmonized for ecosystem types relevant to Norwegian climatic and ecological conditions. All flux values were standardized to g CO_2-eq m^{-2} yr^{-1} using GWP_{100} for CH_4 and linked to the identified LU classes through spatial overlays. This step yielded spatially explicit estimates of pre-inundation GHG emissions and sinks across reservoir footprints.

Third, post-development emissions were estimated using the G-res tool, which models reservoir-specific CO_2 and CH_4 fluxes and their temporal dynamics. Net climate impact was then assessed by comparing pre- and post-inundation fluxes, expressed both as cumulative GWP_{100} and as the GHG intensity of electricity generation (g CO_2-eq kWh^{-1}). Uncertainty was addressed through propagation of measurement and model errors, complemented by sensitivity analyses. Finally, results were validated against available independent datasets and previous studies to ensure comparability and robustness.

In the following sections, we provide detailed descriptions of the data sources, preprocessing procedures, classification methods, flux compilation, reservoir modelling, and uncertainty assessments that underpin these three components.

2.1 Land Use and Wetland Mapping

Most Norwegian reservoirs were constructed or utilized from natural lakes before the 1960s and 1970s (Jensen et al., 2021), making it challenging to use modern remote sensing sources to determine pre-development land types. Previous work by Kenwai et al. (2023), utilized high-resolution historical black-and-white aerial imagery from the Norwegian archive (Norge i Bilder) to identify major land types prior to reservoir development. However, this approach struggled to distinguish wetlands from bare land due to the difficulty of delineating wetland boundaries by visual interpretation of monochromatic imagery and the absence of reliable reference data for validating land type classifications. As a result, wetlands were omitted entirely.

Given the critical role wetlands play in carbon storage and GHG fluxes, there is a pressing need to improve their historical identification and integrate this information with existing spatial databases. This would enable a more accurate assessment of the climate impact associated with reservoir development and the loss of these ecologically important ecosystems.

Recent advances in neural networks and deep learning have demonstrated strong potential for handling complex image classification tasks (Lecun et al., 2015), including the identification of subtle land cover types such as wetlands. These methods offer improved accuracy and scalability compared to traditional approaches. However, their performance is highly dependent on the availability of large, high-quality annotated datasets which, in the context of historical imagery and rare ecosystem types, remain limited (Gui et al., 2025; Ran et al., 2025). This scarcity of training data poses a significant challenge to the direct application of deep learning (Christin et al., 2019; Perry et al., 2022).

To address this challenge, we obtained botanical reports from the Natural History Museum at Norwegian University of Science and Technology (NTNU), which included detailed field maps based on both geographical surveys and aerial photography, dating back to the 1960s and 1970s (NTNU, 2025). These reports provide rich information on wetland boundaries, wetland types, and associated soil characteristics within the corresponding areas.

These reports were manually digitized and georeferenced to align with historical aerial imagery from corresponding time periods and locations. Wetland and non-wetland areas were subsequently annotated in each report to produce a high-quality reference dataset. This process enabled the generation of accurate labels directly corresponding to the aerial imagery, resulting in a valuable ground-truth dataset suitable for training and validating neural network models for wetland classification. Additionally, two random locations were selected, and the AR5/FKB land classification dataset was used to extract wetland information. The AR5/FKB dataset, Norway's official high-resolution land cover mapping system, is widely applied in environmental and resource management. In these areas, the wetland class from the dataset was rasterized for subsequent analysis(NIBIO, 2023). To ensure the consistency and accuracy of this supplementary data, verification was conducted to confirm that no significant anthropogenic or natural land-cover changes had occurred in these locations since the time of the aerial imagery. Figure 1 provides an overview of the selected sample sites along with their corresponding annotations.

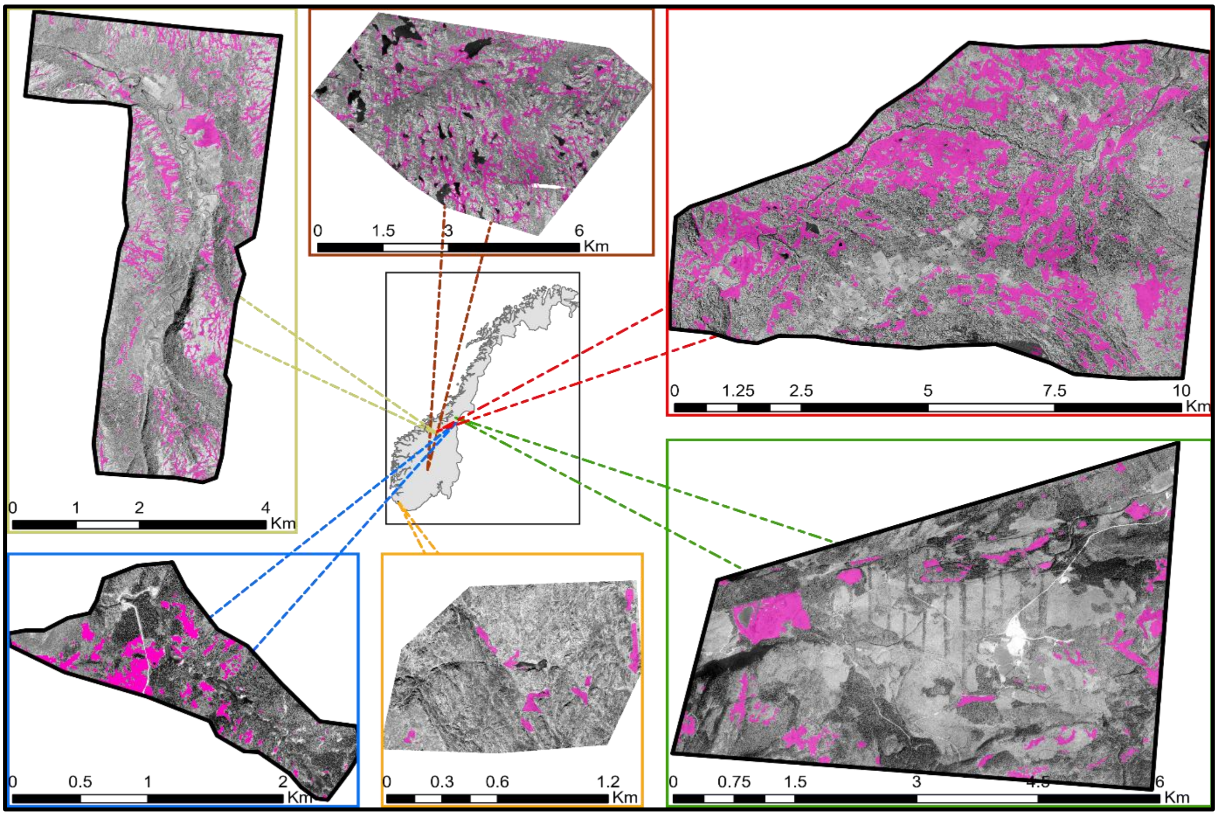

Figure 1: Overview map of the selected sample sites with their corresponding annotations indicating classification results. The pink color represents the areas mapped as wetland areas.

All the labeled rasters, along with their corresponding aerial images, were preprocessed by splitting them into overlapping patches of 512 × 512 pixels. To increase the volume of training data and reduce the risk of overfitting local features, additional patches were generated by augmenting the original patches. The augmentation process was performed by first resampling the original images and the corresponding labels to 1m resolution and applying rotation to 90,180,270 degrees to the original as well as the resampled patches.

Following this, any patches that did not contain wetland information (i.e., patches labeled entirely as non-wetland) were excluded from the dataset to focus the model's learning on relevant features. This preprocessing resulted in a total of 154,482 image patches. These were then divided into 70% for training, 20% for validation, and 10% for testing.

We employed Convolutional Neural Network (CNN) based on the U-Net architecture (Ronneberger et al., 2015), using EfficientNet-B7 as the encoder backbone (Tan & Le, 2019), pre-trained on the ImageNet dataset (Deng et al., 2010). This encoder provided a strong feature extraction capability, especially valuable given the complexity of wetland classification in historical aerial imagery. For data processing, we used GDAL (GDAL/OGR, 2022) for rasterization and resampling, PyTorch (Paszke et al., 2019) for data handling and model implementation, and PyTorch Lightning to enable efficient parallel training across three GPUs. Binary Cross-Entropy (BCE) was used as the loss function, and model performance was evaluated using accuracy, F1 score, and Intersection over Union (IoU) as key metrics.

As CNNs require a substantial amount of training data, the model was initially trained for 100 epochs and then applied to two randomly selected image sets for preliminary mapping. The resulting classification maps were manually refined using expert judgment and visual interpretation as references. These refined outputs were then preprocessed following the same approach described earlier which involves splitting images into overlapping 512×512-pixel patches, resampling, augmenting, and filtering before being added to the original training dataset. This iterative refinement strategy increased the total number of training patches to 228,174, thereby improving the model's learning capacity and generalization performance.

After training the model for 200 epochs, it achieved a training accuracy of 91.1%, an F1 score of 87.9%, and an IoU of 78.6%. For further validation, the model was tested on an independent set of digitized botanical field maps. Using the original field reports as reference, the model achieved an overall accuracy of 88%, demonstrating its reliability and effectiveness in identifying wetland areas from historical aerial imagery. Figure 2 illustrates the workflow of the entire learning process implemented for training the model.

Once the model was validated, it was applied to identify wetland areas within the same dataset used by Kenawi et al. (2023). The classified wetland outputs were then overlaid on the initial thematic raster, in which previously identified land classes were masked out. This masking step was implemented to reduce potential misclassification and improve the overall accuracy of the results by ensuring that only previously unclassified or uncertain areas were subject to wetland detection.

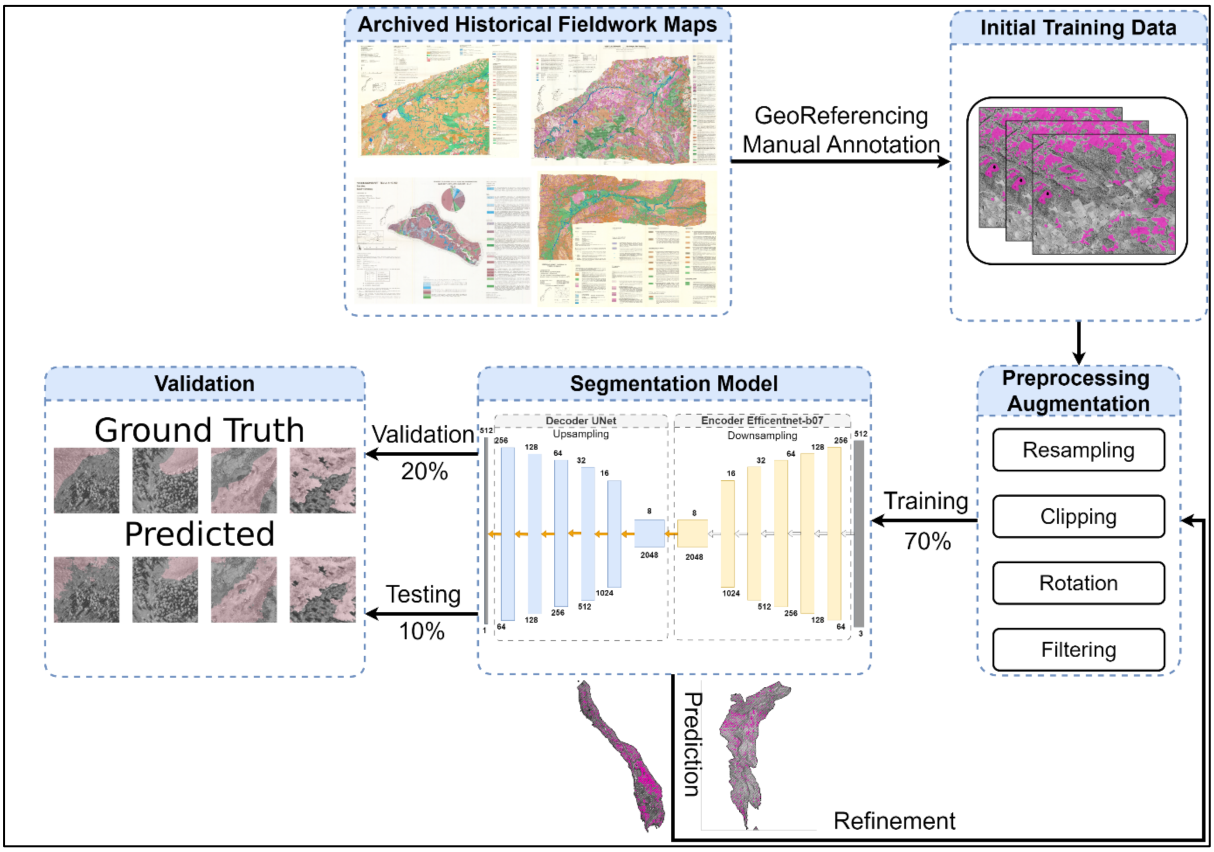

Figure 2: Overview of the deep learning framework used, showing the sequential stages of training, refinement, testing, and validation. The workflow highlights the iterative process of generating preliminary classification maps, manual refinement, preprocessing, integration into training dataset, and subsequent evaluation on independent field maps.

2.2 Ecosystem GHG Flux Data

To associate the identified LU types with potential GHG emissions or sequestration prior to reservoir development, it was necessary to quantify annual fluxes expressed as CO_2-equivalents per ecosystem type. For this purpose, a targeted literature review was conducted to compile representative estimates of NEE and CH_4 fluxes for the ecosystem categories identified in the study LU data.

Given the scope of this study, the review was restricted to the two ecosystem types most relevant to reservoir development impacts in the boreal regions: wetlands and forests. To ensure ecological and climatic relevance, only studies conducted within boreal climatic conditions were considered. Therefore, the review was limited to flux studies representative of such ecosystems.

The available open-access databases of GHG flux measurements (Delwiche et al., 2021; Pastorello et al., 2020; A.-M. Virkkala et al., 2022; A. M. Virkkala et al., 2021) were utilized and filtered to retain only values relevant to this study. In addition, standalone measurements from individual studies were compiled and duplicates were removed (Supplementary Material). All flux values were standardized to a common unit of g C m^{-2} yr^{-1} for both CO_2 and CH_4. As many of the underlying studies also reported site-specific characteristics, additional filtering was performed to distinguish fluxes by ecosystem subtypes. For wetlands, measurements were separated into bogs and fens, while for forests we distinguished between mineral soils, organic soils, and mineral soils with a limited organic layer.

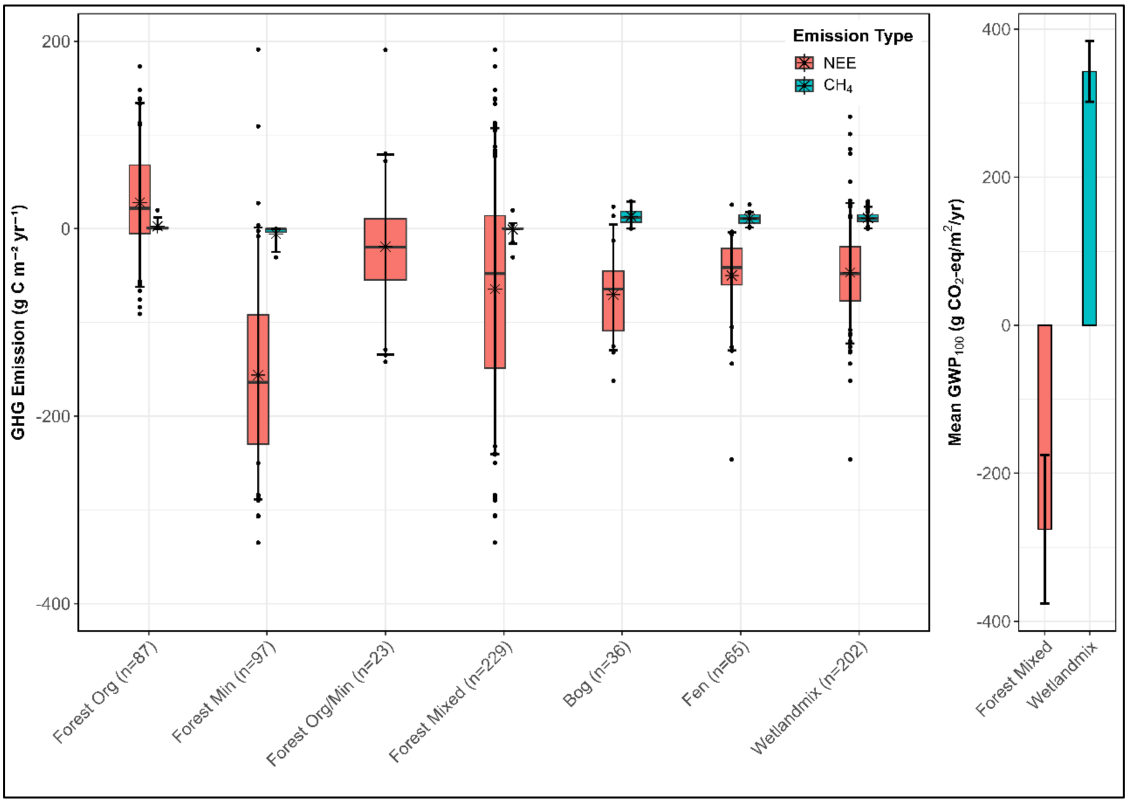

Figure 3: Boxplots of aggregated GHG fluxes for different forest and wetland ecosystems (g C m $^{-2}$ yr $^{-1}$). In addition, the overall GWP values for the two main ecosystem types; forest and wetland are shown in g CO_2-eq m $^{-2}$ yr $^{-1}$.

Following this filtering, measurements were aggregated into two categories: "wetland mix" and "forest mix," each representing combined flux estimates of NEE and CH_4 across their respective subtypes. These aggregated fluxes were then converted into CO_2-equivalents by applying GWP_{100} values for CO_2 and CH_4 as reported by the IPCC. Each ecosystem type was thus assigned a single representative GHG flux in g CO_2-eq m^{-2} yr^{-1}, which was subsequently used in the pre-development emission calculations (Fig. 3).

The annual pre-development emissions for each reservoir footprint were then estimated by multiplying the surface area of each ecosystem type by its representative GWP_{100} value (in g CO_2-eq m^{-2} yr^{-1}). Formally, this can be expressed as:

$$E_{pre} = \sum_{i=1}^{n} (A_i \times F_i)$$

where E_{pre} is the total annual pre-development emission (g CO_2-eq yr), A_i is the surface area of ecosystem type i (m^2), and F_i is the representative annual flux of that ecosystem type (g CO_2-eq m^{-2} yr^{-1}).

To enable comparison with reservoir emissions over a 100-year assessment horizon, the annual pre-development emission rates were multiplied by 100 years. This approach follows the IPCC GWP_{100} standard, allowing direct comparison between the hypothetical scenario of no reservoir development and the modeled post-development emission trajectories.

2.3 Post development reservoir emissions

To evaluate the net GHG emissions resulting from reservoir development, it is necessary to first estimate the annual emissions generated by these reservoirs after construction and then compare these values with the pre-development situation. To achieve this, we relied on the G-res tool, an empirical modeling framework specifically designed to quantify reservoir-related GHG emissions (Prairie et al., 2017).

The G-res tool was developed to integrate multiple types of reservoir and environmental data to predict both pre- and post-reservoir annual emission balances, as well as long-term emissions expressed as GWP_{100}. It incorporates processes such as carbon decomposition, CH_4 production under anaerobic conditions, and other biogeochemical transformations that occur when land is inundated. Its outputs include annual estimates of CO_2, CH_4, and N_2O emissions, along with cumulative GWP_{100}, enabling direct comparisons across reservoirs and land cover types.

To perform these simulations, the G-res tool requires detailed input data, including reservoir morphometry and age, pre-flood land cover, catchment characteristics, and climatic parameters. Reservoir morphometry and age include surface area, depth, volume, and the time since reservoir creation. Pre-flood land cover refers to the vegetation and soil types that were inundated. Catchment characteristics encompass size, land cover, and hydrological inputs to the reservoir. Climatic parameters, such as mean temperature, wind speed, and other relevant local variables, are required to accurately model the biogeochemical processes influencing GHG emissions.

As the primary focus in this study was on LUC associated with reservoir development, the use of G-res was limited to the module related to LUC emissions, excluding emissions from construction or operational activities. Pre-development emission values were derived from a literature review, using published estimates standardized per m^2 per year for different ecosystem types.

The input data for the G-res analysis were compiled from multiple sources to ensure accuracy and spatial consistency. Reservoir morphometry and age were obtained from the NVE Atlas (NVE, 2023), a comprehensive database provided by the Norwegian Water Resources and Energy Directorate (NVE). Pre-flood land cover data were taken from Kenawi et al. (2022) and supplemented with own modeled estimates of wetland areas for each reservoir. Catchment boundaries were generated using NEVINA (NEVINA, 2025), an online portal capable of automatically delineating catchments for specified reservoir locations. Climatic parameters were extracted and matched to each reservoir: long-term mean temperature and precipitation were obtained from the SEKLIMA long-term meteorological database for Norway (MET Norway, 2023). Wind speed was derived from NVE's gridded wind dataset. All variables were spatially joined with the reservoir locations and extracted accordingly (NVE, 2023).As the G-res tool includes its own pre-impoundment assessment module, we also estimated pre-development conditions using our compiled input data within G-res estimated emission factors for boreal regions in order to compare these with our calculated pre-assessment over GWP_{100} horizon as described in section 2.2. This allowed us to evaluate differences in GHG balance depending on whether pre-development conditions are derived from G-res defaults or from our own characterization. Due to the lack of detailed soil type information, particularly for forest ecosystems, we evaluated three scenarios: (i) assuming mineral soils, (ii) assuming organic soils, and (iii) applying our own characterization factors. The results of the post-development GHG assessment for each reservoir were then compared with the estimated pre-development emissions. Comparisons were made for both annual emissions (t CO_2-eq per reservoir per year) and GWP_{100} (kt CO_2-eq per reservoir). Two key perspectives were used to present these comparisons:

2.3.1 GWP 100 Net Emission

We calculated the net 100-year emissions for each reservoir using the equation:

$$Net\ Emission = (E2 - E1) * 100$$

where E2 is the post-development annual emission and E1 is the pre-development annual emission. Multiplication by 100 reflects the cumulative emissions over a 100-year period (GWP_{100}). In addition to our own pre-development estimates, we performed the same comparison using G-res default assessments under three scenarios: mineral soils, organic soils, and our own characterization factors. This approach provides a direct quantification of the net effect of reservoir creation on long-term GHG balance.

2.3.2 Emission Intensity

To link reservoir emissions with hydropower generation, each reservoir was associated with its corresponding hydropower system following the mapping framework of Kenawi et al. (2025). Since Norwegian HP systems often operate in cascades, where multiple reservoirs are connected to one or more power plants, we, a surface-area weighting factor was applied to proportionally allocate emissions similarly to what have been implemented by Kenawi et al. (2025). Reservoir-specific net emissions were then normalized by the allocated annual electricity production of each HP system, yielding system-level GHG intensities expressed as g CO_2-eq per kWh.

3 Results

A total of 52 reservoirs were analyzed to identify their LU–related emission pathways, with surface areas ranging from 0.1 to 64 km^2. Detailed results on LUC, annual pre-development emissions, 100-year GWP_{100}, and emission intensity are presented below.

3.1 Land Use Change

We quantified and distinguished wetland areas from the original dataset of Kenawi et al. (2022) for the analyzed reservoirs and overlaid them on the existing LU data. Wetland areas varied considerably across reservoirs (Fig. 4), ranging from 0 to 17 km^2. The total identified wetland area was estimated to 103 km^2, slightly larger than the previously identified vegetation area of 88 km^2. On average, wetlands accounted for 20% of the total analyzed land and an average of 18% per single reservoir.

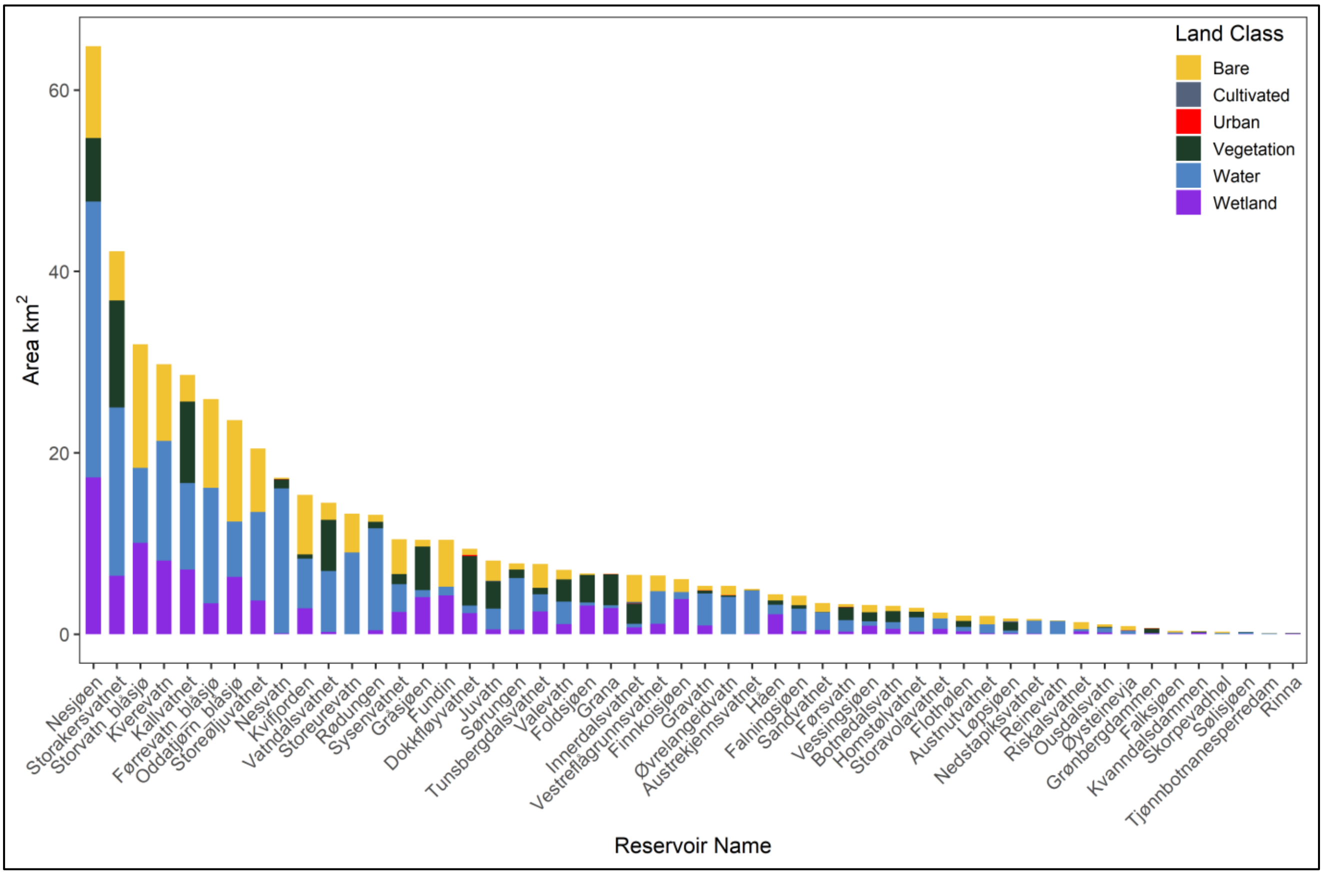

Figure 4: Overview of total LU in the analyzed reservoirs after integrating the wetland class into the original dataset.

3.2 Annual Pre Development Emission

We associated the identified LU prior to the development of each analyzed reservoir with the estimated net carbon flux for each ecosystem type, including wetlands and forests. Net annual emissions (t CO_2 eq yr^{-1}) varied across reservoirs (Fig. 5), depending on their land composition and total surface area. Net annual pre-development emissions ranged from −1,470 to 3,981 t CO_2 eq yr^{-1}, with an average of 306 t CO_2 eq yr^{-1}. Negative values indicate net carbon sequestration, whereas positive values represent net carbon emissions.

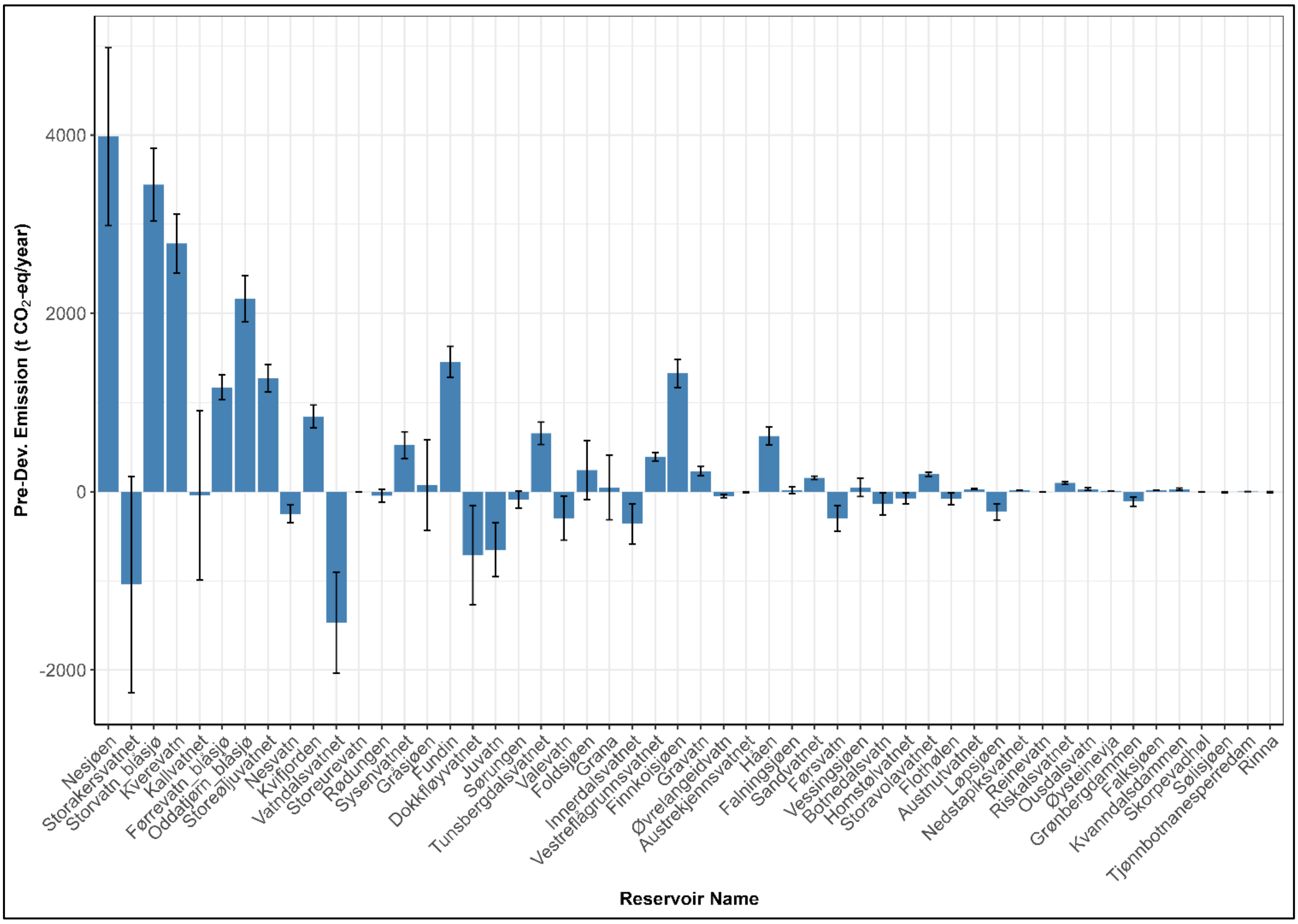

Figure 5: Overview of annual pre-development emissions (t CO_2-eq yr^{-1}) for our analyzed reservoirs based on estimated ecosystem GWP values.

3.3 GWP100 Net Emission

We quantified the net GWP_{100} for all analyzed reservoirs under three main scenarios: our own estimates, G-res assuming mineral soils, and G-res assuming organic soils (Fig. 6). The results revealed a clear dependence on the pre-impoundment baseline assumption. Under the organic soil scenario, most reservoirs acted as net carbon sinks, with negative GWP_{100} values. In contrast, both the mineral soil scenario and our own estimates generally show reservoirs as net carbon sources, yielding positive GWP_{100} values for the majority of cases.

Additionally, Figure 7 illustrates the spatial distribution of net GWP_{100} across Norwegian reservoirs, highlighting substantial variability among sites. Total net estimates ranged from a minimum of –260 kt CO_2-eq (indicating a strong sink effect) to a maximum of 217 kt CO_2-eq (indicating a strong source effect). This wide range emphasizes that the climate impact of reservoir development is highly site-specific and sensitive to assumptions regarding pre-flood soil and land cover characteristics.

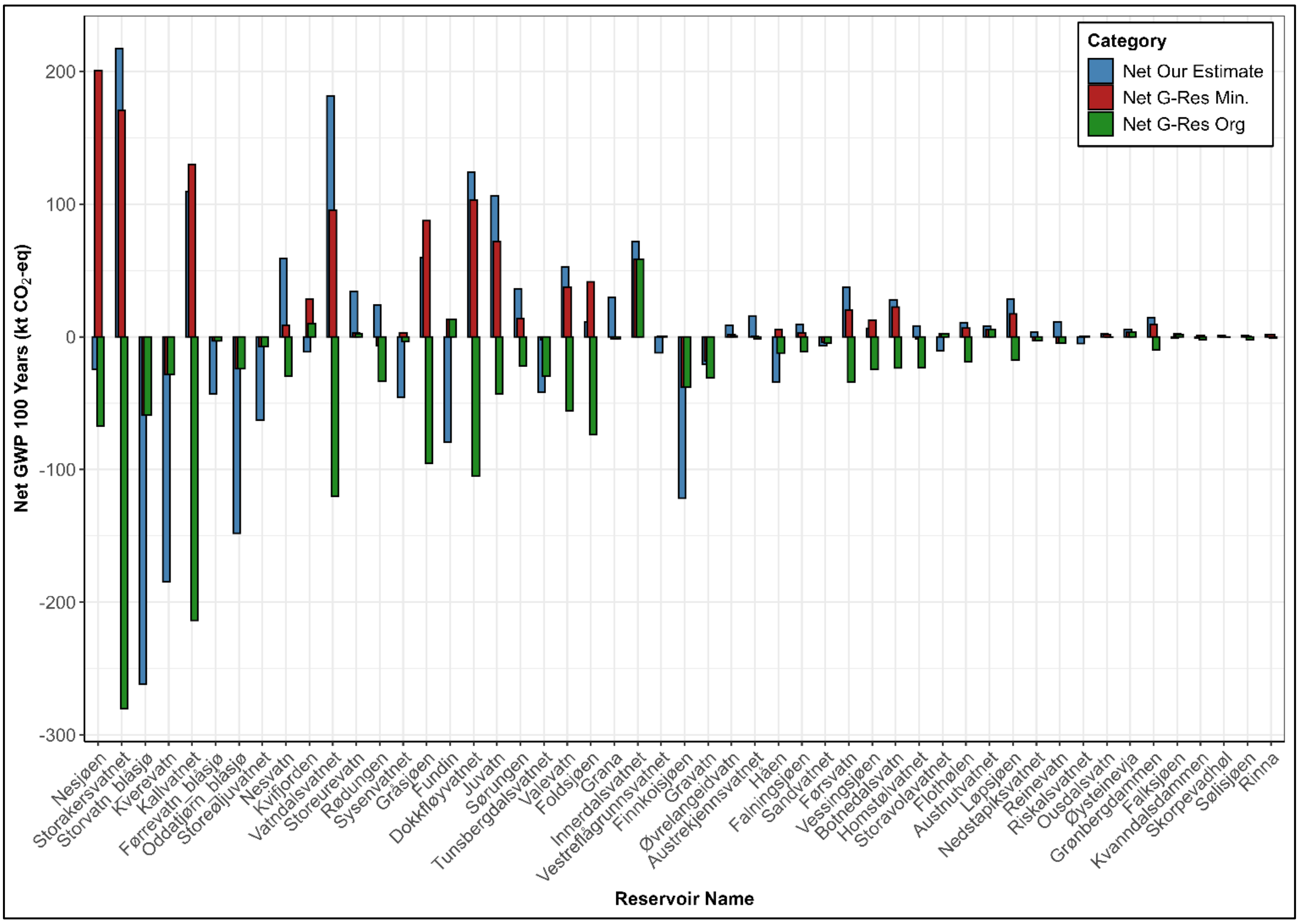

Figure 6: Comparison of net GWP_{100} emissions per reservoir (kt CO_2-eq) based on our estimates and two G-res scenarios, considering both mineral (Min) and organic (Org) soil conditions.

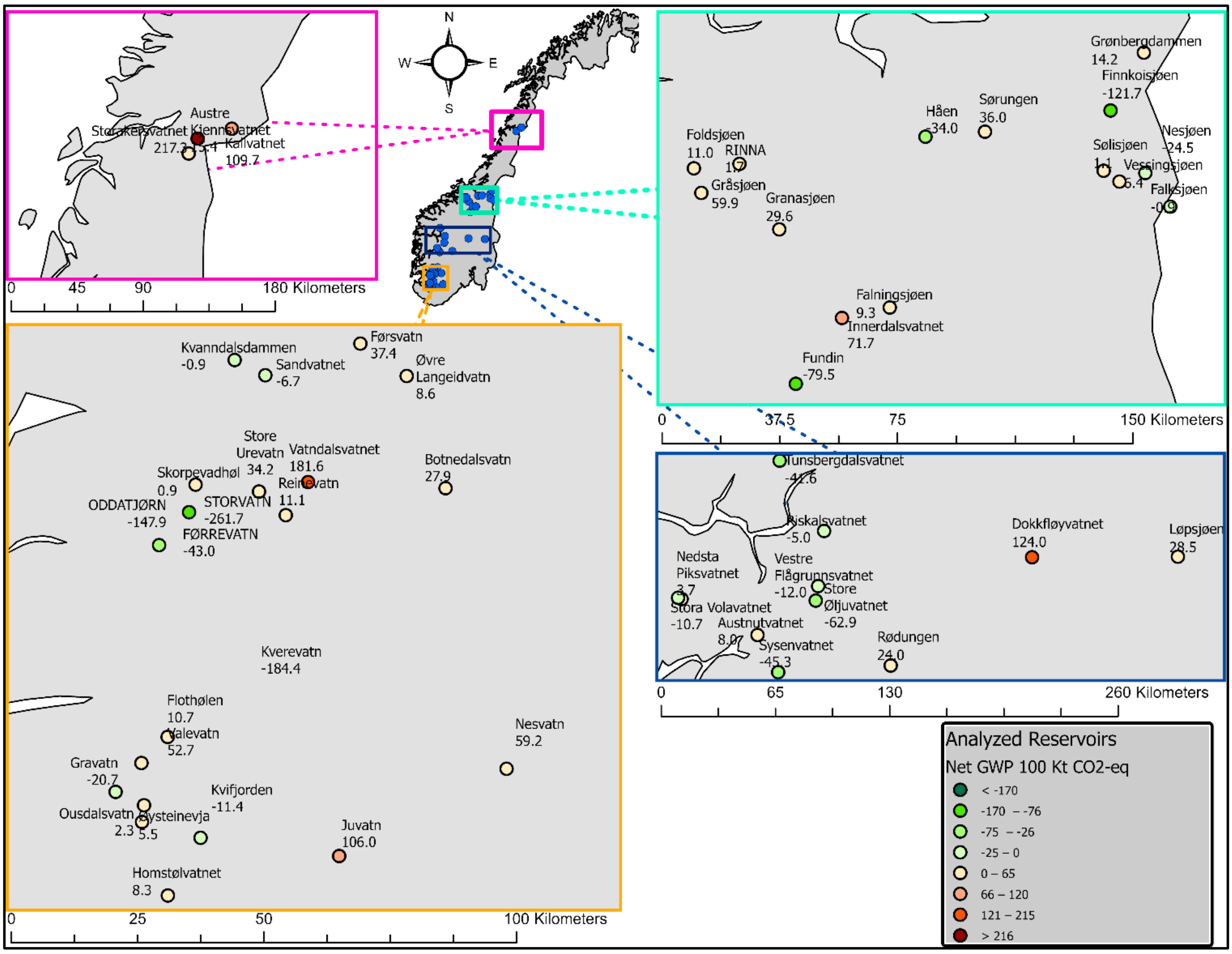

Figure 7: Spatial distribution of net GWP_{100} emissions from the analyzed reservoirs across Norway.

3.4 Emission Intensity

The analyzed reservoirs were associated with their respective hydropower systems and the corresponding annual electricity production. Results show that emission intensity varied substantially across systems (Fig. 8), ranging from –7 to 4 g CO_2-eq/kWh. Negative values indicate cases where reservoirs acted as net carbon sinks relative to energy production, while positive values reflect systems functioning as net emission sources. When aggregated across all systems, the mean emission intensity from land use change due to the inundation of the land only was 0.19 g CO_2-eq/kWh.

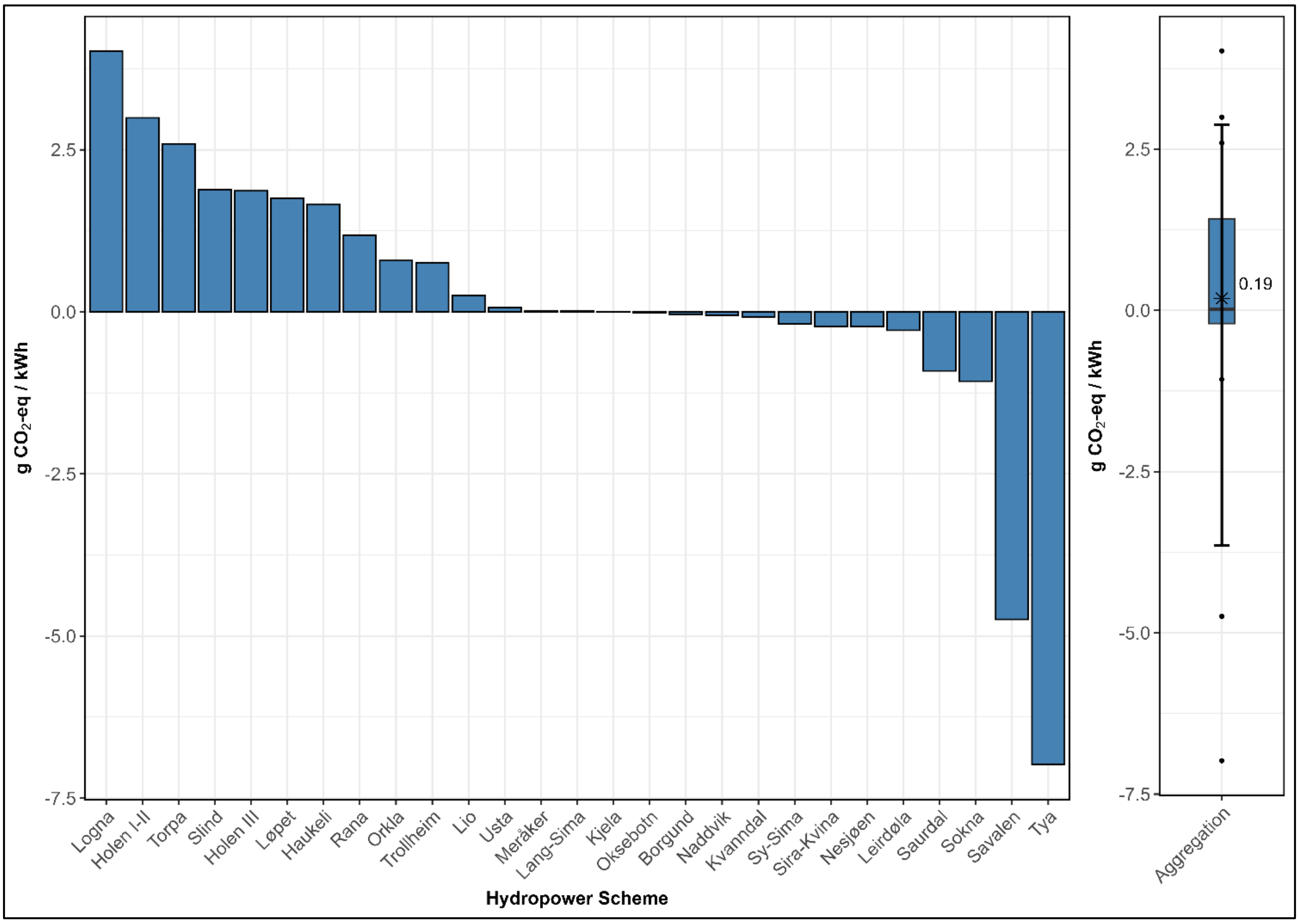

Figure 8: Emission intensity (g CO_2-eq kWh $^{-1}$) of hydropower systems associated with the analyzed reservoirs, including the overall aggregation shown as a boxplot.

4 Discussion

The dynamics between GHG emissions and reservoir impoundment remain highly uncertain, often leading to systematic over- or underestimation (Kumar et al., 2023). In this study, these uncertainties were addressed by integrating remote sensing data, deep learning–based classification, and ecosystem service assessments to evaluate the net emissions of 52 reservoirs in Norway, taking into account pre-impoundment emissions and using the G-res tool to quantify post-development emissions, enabling a more robust calculation of the net GHG balance. Furthermore, these emissions were associated with the electricity generated by the corresponding hydropower systems, providing direct insights into the emission intensity of Norwegian hydropower production.

The use of CNNs proved highly efficient for classifying complex land cover types that are difficult to distinguish by human interpretation, particularly in historical black-and-white aerial imagery. Our model was further validated on independent botanical field maps, achieving an overall accuracy of 88%, which demonstrates its robustness for external deployment. Wetlands accounted for 103 km^2 of the pre-flooded area, representing about 20% on average across the analyzed reservoirs. This extent was slightly larger than the previously identified vegetation area of 88 km^2, underscoring the substantial role of wetlands in shaping pre-impoundment carbon dynamics. By incorporating wetlands into the dataset, our analysis provides a more reliable basis for estimating pre-development emissions and evaluating the net climate impact of reservoir creation.

The aggregation of wetlands ecosystem GWP_{100} values reveal that wetlands, despite their high carbon sequestration capacity (171 ± 17 g CO_2-eq m^{-2} yr^{-1}), they function as net GHG sources overall, with a mean emission of 342 ± 40 g CO_2-eq m^{-2} yr^{-1}. This imbalance is primarily attributed to elevated CH_4 fluxes, which significantly outweigh CO_2 uptake when expressed in CO_2-equivalents. These findings align with broader observations across boreal wetland systems (Helbig et al., 2017; Kuhn et al., 2025; Yuan et al., 2024) and highlight the critical role of CH_4 in driving net radiative forcing from these landscapes. Nonetheless, it is essential that such outcomes are not interpreted in isolation. Wetlands remain vital to the stability of the global carbon cycle (Olefeldt et al., 2021) and biodiversity conservation (Conlisk et al., 2023; Schindler & Lee, 2010). Their exclusion from carbon accounting frameworks risks undermining the complexity of their ecological functions. Therefore, future management strategies should balance climate mitigation goals with the preservation of wetland ecosystem services.

Pre-development emission rates varied widely from a sequestration of –1,470 t CO_2-eq yr^{-1} to a release of 3,981 t CO_2-eq yr^{-1}, with a mean of 306 t CO_2-eq yr^{-1}. This variability highlights the importance of accurately characterizing pre-impoundment conditions, as they strongly influence the estimated net climate effect of reservoir creation. When comparing our pre-development estimates with those generated by the G-res tool, notable differences emerged depending on baseline assumptions. In particular, scenarios assuming organic soils often suggested reservoirs functioned as net carbon sinks, with net GWP_{100} values as low as –260 kt CO_2-eq, whereas mineral soil assumptions and our own characterization generally indicated net carbon sources, with values up to 217 kt CO_2-eq. This contrast illustrates the sensitivity of long-term GHG assessments to pre-flood land cover and soil properties, underlining the need for site-specific data to avoid systematic over- or underestimation of reservoir emissions.

Consequently, our analysis indicates that the GHG emission intensities of the sampled Norwegian reservoirs are lower than many previous estimates (Modahl & Raadal, 2015). This finding supports observations that current estimates are likely inflated due to the application of global or tropical emission factors that do not reflect boreal conditions (NTNU, 2025). Importantly, we used aggregated literature-based emission factors that provide greater detail and specificity than the broader boreal coefficients applied by the G-Res tool.

Despite these advances, several limitations introduce uncertainty. A key issue is the resolution of pre-impoundment data. While field data differentiates the carbon dynamics of bogs (sinks) and fens (emitters), our remote sensing classification could not make this distinction. Furthermore, we were unable to characterize sublayer soil types beneath forests, requiring data aggregation that can lead to significant estimation errors. As Figure 6 illustrates, the assumption of organic vs. mineral soil dramatically alters the results, highlighting this sensitivity.

A second limitation stems from the modeling tools themselves. The G-Res tool is an empirical model based on aggregated data and is designed for typical reservoirs. It cannot adequately capture the dynamics of converting natural lakes to reservoirs, forcing us to exclude such systems from our analysis. More advanced, process-based models could provide a deeper understanding but require extensive input data on soil and ecosystem properties that were unavailable for this study, contributing to the overall uncertainty.

Notwithstanding these limitations, this study provides a refined estimate of GHG emissions from Norwegian reservoirs. Our work underscores the necessity for additional field data collection and the development of advanced modeling tools capable of simulating ecosystem emissions before and after impoundment. Such efforts are critical for improving the reliability of emission estimates and supporting informed decision-making in the hydropower sector.

5 Conclusion

This study provides a refined estimate of the net GHG impact of Norwegian reservoirs by integrating remote sensing, deep learning, and empirical modeling. Including wetlands in the land use classification significantly improved pre-development emission estimates, showing that these ecosystems play a key role in shaping the carbon balance of reservoir areas. The CNN-based classification achieved 88% accuracy, identifying wetlands as about 20% of pre-flooded land. When compared with G-res default scenarios, results showed that assumptions about soil type and pre-flood conditions strongly influence GHG outcomes. On average, Norwegian reservoirs had a low emission intensity of 0.19 g CO_2-eq kWh^{-1}, confirming that hydropower under boreal conditions contributes minimally to life-cycle emissions. Although uncertainties remain, particularly regarding soil data and model simplifications, this study highlights the need for continued development of tools, datasets, and modeling approaches to better understand the complex relationship between reservoirs and their GHG emissions.

ACKNOWLEDGMENTS

This work is part of the project Footprint and Impacts of Renewable Energy: Pressure on Lands Under Growth (FIREPLUG). The project was funded by the Research Council of Norway (RCN) number 319925. All figures and tables presented in this work have been created by the author. No permission from other sources is required.

AUTHOR CONTRIBUTIONS

Conceptualization: Kenawi MS

Methodology: Kenawi MS, Silvennoinen HM

Data curation: Kenawi MS, Silvennoinen HM

Formal analysis: Kenawi MS, Vakhidi F, Gotsiridze E

Supervision: Sandercock BK, Bakken TH, Alfredsen K, Silvennoinen HM

Writing – original draft: Kenawi MS

Writing – review & editing: All authors.

CONFLICT OF INTEREST

The authors declare that they have no conflict of interest.

List of Abbreviations

GHG: Greenhouse Gas

LU: Land Use

LUC: Land Use Change

CO_2: Carbon Dioxide

CH_4: Methane

GWP_{100}: 100-year Global Warming Potential

GWP: Global Warming Potential

CNN: Convolutional Neural Network

BCE: Binary Cross-Entropy

IoU: Intersection over Union

NEE: Net Ecosystem Exchange

NVE: Norwegian Water Resources and Energy Directorate

NTNU: Norwegian University of Science and Technology

AR5/FKB: Arealressurskart / Felles Kartbase (Norwegian Land Cover Dataset)

GDAL: Geospatial Data Abstraction Library

G-Res: Greenhouse Gas Reservoir Tool

NEVINA: NVE’s Catchment Delineation Portal

SEKLIMA: Norwegian Meteorological Database

IPCC: Intergovernmental Panel on Climate Change

HP: Hydropower

OBIA: Object-Based Image Analysis

Kt: Kiloton

t CO_2-eq: Tonnes of Carbon Dioxide Equivalent

g CO_2-eq/kWh: Grams of Carbon Dioxide Equivalent per Kilowatt-hour

References

Bertassoli, D. J., Sawakuchi, H. O., De Araújo, K. R., De Camargo, M. G. P., Alem, V. A. T., Pereira, T. S., Krusche, A. V., Bastviken, D., Richey, J. E., & Sawakuchi, A. O. (2021). How green can Amazon hydropower be? Net carbon emission from the largest hydropower plant in Amazonia. *Science Advances*, *7*(26). https://doi.org/10.1126/SCIADV.ABE1470/SUPPL_FILE/ABE1470_SM.PDF

Christin, S., Hervet, É., & Lecomte, N. (2019). Applications for deep learning in ecology. *Methods in Ecology and Evolution*, *10*(10), 1632–1644. https://doi.org/10.1111/2041-210X.13256

Conlisk, E., Chamberlin, L., Vernon, M., & Dybala, K. E. (2023). *Evidence for the Multiple Benefits of Wetland Conservation in North America: Carbon, Biodiversity, and Beyond With funding from Natural Resources Defense Council*. https://doi.org/10.5281/zenodo.7388321

Delwiche, K. B., Knox, S. H., Malhotra, A., Fluet-Chouinard, E., McNicol, G., Feron, S., Ouyang, Z., Papale, D., Trotta, C., Canfora, E., Cheah, Y. W., Christianson, D., Alberto, M. C. R., Alekseychik, P., Aurela, M., Baldocchi, D., Bansal, S., Billesbach, D. P., Bohrer, G., … Jackson, R. B. (2021). FLUXNET-CH4: A global, multi-ecosystem dataset and analysis of methane seasonality from freshwater wetlands. *Earth System Science Data*, *13*(7), 3607–3689. https://doi.org/10.5194/essd-13-3607-2021

Deng, J., Dong, W., Socher, R., Li, L.-J., Kai Li, & Li Fei-Fei. (2010). *ImageNet: A large-scale hierarchical image database*. 248–255. https://doi.org/10.1109/CVPR.2009.5206848

GDAL/OGR contributors. (2022). *{GDAL/OGR} Geospatial Data Abstraction software Library*. https://doi.org/10.5281/zenodo.5884351

Gui, Y., Li, W., Xia, X. G., Eben, B., Ginzler, C., & Wang, Z. (2025). Mapping Countrywide Historical Tree Cover Using Semantic Segmentation. *IEEE Transactions on Geoscience and Remote Sensing*, *63*. https://doi.org/10.1109/TGRS.2025.3532248

Helbig, M., Chasmer, L. E., Kljun, N. C., Quinton, W. L., Treat, C. C., & Sonnentag, O. (2017). The positive net radiative greenhouse gas forcing of increasing methane emissions from a thawing boreal forest-wetland landscape. *Global Change Biology*, *23*(6), 2413–2427. https://doi.org/10.1111/gcb.13520

IEA. (2021). *Renewables - Fuels & Technologies - IEA*. https://www.iea.org/fuels-and-technologies/renewables

IPCC. (2022). Impacts, Adaptation, and Vulnerability. Working Group II Contribution to the IPCC Sixth Assessment Report of the Intergovernmental Panel on Climate Change; Pötner, H. In *O., Roberts, DC, Tignor, M., Poloczanska, ES, Mintenbeck, K., Ale, A., Eds*. https://doi.org/10.1017/9781009325844.Front

Jensen, T., Stensby, K. E., Vognild, I. H., & Brittain, J. E. (2021). *Norway ' s hydroelectric development* (Issue 28).

Jia, G., Shevliakova, E., Artaxo, P., De Noblet-Ducoudré, N., Houghton, R., House, J., Kitajima, K., Lennard, C., Popp, A., Sirin, A., Sukumar, R., Verchot, L., Anderegg, W., Armstrong, E., Bastos, A., Bernsten, T. K., Cai, P., Calvin, K., Cherubini, F., ... Verchot, L. (2022). Land-climate interactions. In *Climate Change and Land: An IPCC Special Report on climate change, desertification, land degradation, sustainable land management, food security, and greenhouse gas fluxes in terrestrial ecosystems* (pp. 131–247). https://doi.org/10.1017/9781009157988.004

Kenawi, M. S., Alfredsen, K., Stürzer, L. S., Sandercock, B. K., & Bakken, T. H. (2023). High-resolution mapping of land use changes in Norwegian hydropower systems. *Renewable and Sustainable Energy Reviews*, *188*, 113798. https://doi.org/10.1016/J.RSER.2023.113798

Kuhn, M., Olefeldt, D., Arndt, K. A., Bastviken, D., Bruhwiler, L., Crill, P., DelSontro, T., Fluet-Chouinard, E., Grosse, G., Hovemyr, M., Hugelius, G., MacIntyre, S., Malhotra, A., McGuire, A. D., Oh, Y., Poulter, B., Treat, C. C., Turetsky, M. R., Varner, R. K., … Zhang, Z. (2025). Current and future methane emissions from boreal-Arctic wetlands and lakes. *Nature Climate Change*, *15*(9), 986–991. https://doi.org/10.1038/s41558-025-02413-y

Kumar, A., Kumar, A., Chaturvedi, A. K., Joshi, N., Mondal, R., & Malyan, S. K. (2023). Greenhouse gas emissions from hydroelectric reservoirs: mechanistic understanding of influencing factors and future prospect. *Environmental Science and Pollution Research*, *1*, 1–18. https://doi.org/10.1007/S11356-023-25717-Y/TABLES/3

Lecun, Y., Bengio, Y., & Hinton, G. (2015). Deep learning. *Nature 2015 521:7553*, *521*(7553), 436–444. https://doi.org/10.1038/nature14539

Li, S., & Zhang, Q. (2014). Carbon emission from global hydroelectric reservoirs revisited. *Environmental Science and Pollution Research*, *21*(23), 13636–13641. https://doi.org/10.1007/S11356-014-3165-4/FIGURES/1

MET Norway. (2023). *Observations and weather statistics - Seklima*. The Norwegian Meteorological Institute. https://seklima.met.no/

Modahl, I. S., & Raadal, H. L. (2015). *The inventory and life cycle data for Norwegian hydroelectricity* (Issue 2012).

NEVINA. (2025). *NEVINA*. https://nevina.nve.no/?trk=public_post-text

NIBIO. (2023). *AR5 - NIBIO*. https://www.nibio.no/tema/jord/arealressurser/arealressurskartar5

NTNU. (2025). *Vitenskapsmuseet: Botanisk rapport - NTNU*. https://www.ntnu.no/museum/botaniske-og-zoologiske-rapporter

NVE. (2023). *NVE Atlas 3.0*. https://atlas.nve.no/Html5Viewer/index.html?viewer=nveatlas#

OED. (2022). *Norway's Resource Report 2022*. https://www.sodir.no/en/whats-new/publications/reports/resource-report/resource-report-2022/

Olefeldt, D., Hovemyr, M., Kuhn, M. A., Bastviken, D., Bohn, T. J., Connolly, J., Crill, P., Euskirchen, E. S., Finkelstein, S. A., Genet, H., Grosse, G., Harris, L. I., Heffernan, L., Helbig, M., Hugelius, G., Hutchins, R., Juutinen, S., Lara, M. J., Malhotra, A., … Watts, J. D. (2021). The boreal-arctic wetland and lake dataset (BAWLD). *Earth System Science Data*, *13*(11), 5127–5149. https://doi.org/10.5194/ESSD-13-5127-2021

Pastorello, G., Trotta, C., Canfora, E., Chu, H., Christianson, D., Cheah, Y. W., Poindexter, C., Chen, J., Elbashandy, A., Humphrey, M., Isaac, P., Polidori, D., Ribeca, A., van Ingen, C., Zhang, L., Amiro, B., Ammann, C., Arain, M. A., Ardö, J., … Papale, D. (2020). The FLUXNET2015 dataset and the ONEFlux processing pipeline for eddy covariance data. *Scientific Data 2020 7:1*, *7*(1), 1–27. https://doi.org/10.1038/s41597-020-0534-3

Paszke, A., Gross, S., Massa, F., Lerer, A., Bradbury, J., Chanan, G., Killeen, T., Lin, Z., Gimelshein, N., Antiga, L., Desmaison, A., Köpf, A., Yang, E., DeVito, Z., Raison, M., Tejani, A., Chilamkurthy, S., Steiner, B., Fang, L., … Chintala, S. (2019). PyTorch: An Imperative Style, High-Performance Deep Learning Library. *Advances in Neural Information Processing Systems*, *32*. https://arxiv.org/abs/1912.01703v1

Perry, G. L. W., Seidl, R., Bellvé, A. M., & Rammer, W. (2022). An Outlook for Deep Learning in Ecosystem Science. *Ecosystems*, *25*(8), 1700–1718. https://doi.org/10.1007/S10021-022-00789-Y/FIGURES/4

Prairie, Y. T., Alm, J., Harby, A., Mercier-Blais, S., & Nahas, R. (2017). *The GHG Reservoir Tool (G-res), UNESCO/IHA research project on the GHG status of freshwater reservoirs*.

Ran, S., Ma, G., Chi, F., Zhou, W., & Weng, Y. (2025). HPM-Match: A Generic Deep Learning Framework for Historical Landslide Identification Based on Hybrid Perturbation Mean Match. *Remote Sensing 2025, Vol. 17, Page 147*, *17*(1), 147. https://doi.org/10.3390/RS17010147

Rodriguez, M., & Casper, P. (2018). Greenhouse gas emissions from a semi-arid tropical reservoir in northeastern Brazil. *Regional Environmental Change*, *18*(7), 1901–1912. https://doi.org/10.1007/S10113-018-1289-7/FIGURES/4

Ronneberger, O., Fischer, P., & Brox, T. (2015). U-net: Convolutional networks for biomedical image segmentation. *Lecture Notes in Computer Science (Including Subseries Lecture Notes in Artificial Intelligence and Lecture Notes in Bioinformatics)*, *9351*, 234–241. https://doi.org/10.1007/978-3-319-24574-4_28/COVER

Schindler, D. W., & Lee, P. G. (2010). Comprehensive conservation planning to protect biodiversity and ecosystem services in Canadian boreal regions under a warming climate and increasing exploitation. *Biological Conservation*, *143*(7), 1571–1586. https://doi.org/10.1016/j.biocon.2010.04.003

Tan, M., & Le, Q. V. (2019). EfficientNet: Rethinking Model Scaling for Convolutional Neural Networks. *36th International Conference on Machine Learning, ICML 2019*, *2019-June*, 10691–10700. https://arxiv.org/abs/1905.11946v5

Virkkala, A.-M., Natali, S. M., Rogers, B. M., Watts, J. D., Savage, K., June Connon, S., Mauritz, M., G Schuur, E. A., Peter, D., Minions, C., Nojeim, J., Commane, R., Emmerton, C. A., Goeckede, M., Helbig, M., Holl, D., Iwata, H., Kobayashi, H., Kolari, P., … Zyryanov, V. I. (2022). The ABCflux database: Arctic-boreal CO 2 flux observations and ancillary information aggregated to monthly time steps across terrestrial ecosystems. *Earth Syst. Sci. Data*, *14*, 179–208. https://doi.org/10.5194/essd-14-179-2022

Virkkala, A. M., Aalto, J., Rogers, B. M., Tagesson, T., Treat, C. C., Natali, S. M., Watts, J. D., Potter, S., Lehtonen, A., Mauritz, M., Schuur, E. A. G., Kochendorfer, J., Zona, D., Oechel, W., Kobayashi, H., Humphreys, E., Goeckede, M., Iwata, H., Lafleur, P. M., ... Luoto, M. (2021). Statistical upscaling of ecosystem CO_2 fluxes across the terrestrial tundra and boreal domain: Regional patterns and uncertainties. *Global Change Biology*, *27*(17), 4040–4059. https://doi.org/10.1111/GCB.15659

Yuan, K., Li, F., McNicol, G., Chen, M., Hoyt, A., Knox, S., Riley, W. J., Jackson, R., & Zhu, Q. (2024). Boreal–Arctic wetland methane emissions modulated by warming and vegetation activity. *Nature Climate Change*, *14*(3), 282–288. https://doi.org/10.1038/s41558-024-01933-3

Supplementary Material

Additional information supporting this study is provided in the supplementary Excel file:

Supplementary Data S1 – Ecosystem Flux Dataset.xlsx